Highly Sensitive Biosensing Using Arrays of Plasmonic Au Nanodisks Realized by Nanoimprint Lithography

Seung-Woo Lee,[†] Kyeong-Seok Lee,[‡] Junhyoung Ahn,[†,⊥] Jae-Jong Lee,[§,⊥] Min-Gon Kim,[†,⊥,*] and Yong-Beom Shin[†,⊥,*]

[†]Korea Research Institute of Bioscience and Biotechnology (KRIBB), 111 Gwahangno, Yuseong-gu, Daejeon 305-806, South Korea, [‡]Korea Institute of Science and Technology (KIST), 39-1 Hawolgok-dongWolsong-gil, 5, Seong-buk-gu, Seoul 136-791, South Korea, [§]Korea Institute of Machinery and Materials (KIMM), 104 Sinseongno, Yuseong-gu, Daejeon 305-343, South Korea, and [⊥]University of Science & Technology (UST), 176 Gajung-dong, Yuseong-gu, Daejeon 305-350, South Korea

ABSTRACT We describe the fabrication of elliptical Au nanodisk arrays as a localized surface plasmon resonance (LSPR) sensing substrate for clinical immunoassay *via* thermal nanoimprint lithography (NIL) and enhancement in the sensitivity of the detection of the prostate-specific antigen (PSA) using the precipitation of 5-bromo-4-chloro-3-indolyl phosphate *p*-toluidine/nitro blue tetrazolium (BCIP/NBT), catalyzed by alkaline phosphatase. Au nanodisks were fabricated on glass through an unconventional tilted evaporation, which could preserve the thickness of imprinted resists and create an undercut beneficial to the subsequent lift-off process without any damage to pattern dimension and the glass while removing the residual polymers. To investigate the optically anisotropic property of the LSPR sensors, a probe light with linear polarization parallel to and perpendicular to the long axis of the elliptical nanodisk array was utilized, and their sensitivity to the bulk refractive index (RI) was measured as 327 and 167 nm/RIU, respectively. To our knowledge, this is the first application of enzyme−substrate reaction to sandwich immunoassay-based LSPR biosensors that previously suffered from a low sensitivity due to the short penetration depth of the plasmon field, especially when large-sized antibodies were used as bioreceptors. As a result, a large change in local refractive index because of the precipitation on the Au nanodisks amplified the wavelength shift of the LSPR peak in the vis−NIR spectrum, resulting in femtomolar detection limits, which was ~10^5-fold lower than the label-free detection without the enzyme precipitation. This method can be extended easily to the other clinical diagnostics with a high sensitivity.

KEYWORDS: nanodisk arrays · nanoimprint lithography · localized surface plasmon resonance · prostate-specific antigen · enzymatic precipitation

Localized surface plasmon resonance (LSPR) sensors have been studied intensively as one of the promising nanobiosensors for medical diagnosis, monitoring of diseases, and the detection of environmental pollutants because of their high sensitivity, label-free detection, low sample volumes, low-cost instruments, and real-time detection.[1−3] In general, the biosensing based on LSPR utilizes a strong extinction band in the vis−NIR range. The extinction originates from the collective oscillation of the conduction electrons in the metal nanoparticle (NP), induced by the incident photons or electrons with the specific resonant energy. The peak wavelength, extinction magnitude of LSPR spectra, and decay length of the LSP field are highly dependent upon the size, shape, interparticle spacing, and composition of noble metal nanostructures.[4−6] Understanding how NP structures affect these LSPR properties, optimizing nanostructure design, and improving their sensitivity/detection limit are important issues of current LSPR biosensor research.[7] In this paper, we focus on the easy fabrication of metallic nanostructures and the enhancement of the LSPR sensitivity to an extremely low limit of detection (LOD).

The desirable nanofabrication technique for substrate-bound nanostructures would have some of the conspicuous features, including low-cost fabrication, large-area patterning, reproducibility, and tunability of their optical properties. For this reason, unconventional approaches to nanofabrication such as soft nanoimprint lithography,[8,9] nanosphere lithography (NSL),[10,11] colloidal lithography,[12] nanoimprint lithography (NIL),[13] and solution-phase synthesis[14,15] appear to be far preferable to conventional approaches, like e-beam lithography and focused ion beam lithography. Soft nanoimprint lithography has been used to develope a class of quasi-3D plasmonic crystal that consists of multilaryered, regular arrays of subwavelength metal nanostructures. Their quasi-3D nanostructures were fabricated by depositing Au on the imprinted surface of a polymer, resulting with the plasmonic response being represented in a combination of LSPR response and Bloch wave resonances.[8,9] NSL is one of the most widely used techniques because it can produce large-scale biosensor arrays with a simple fabrication process. This technique utilizes a hexagonally close-packed nanosphere mask that permits direct metal

*Address correspondence to ybshin@kribb.re.kr, mgkim@kribb.re.kr.

Received for review August 16, 2010 and accepted January 3, 2011.

Published online January 11, 2011
10.1021/nn102041m

deposition onto a substrate through the interstitial regions of the mask. The formation of the close-packed nanoshere arrays is the most critical step in NSL to produce well-ordered and uniform nanostructures.[10,11] Of course, it should be noted that inherent limitations of NSL include the defective formation of nanosphere arrays and its limited pattern design.[12,13] Recently, NIL was proposed as an alternative technique that can not only overcome the limitations of NSL but also produce marketable LSPR sensors.[13] It is well-known that NIL is a stamp-based, low-cost, and high-throughput lithographic method that can generate largely nanopatterned areas with sub-10 nm resolution.[16] Despite its great potential, however, practical applications of NIL as a nanofabrication method for the LSPR sensors have been rarely reported so far. This is probably attributed to two constraints on NIL: (a) fabrication of a large-area stamp with high feature density,[17] and (b) development of a highly efficient process for a successful pattern transfer.[18]

In general, the LSPR sensitivity to the bulk RI is much lower because of the shorter decay length of the plasmon field than in SPR, the so-called propagating surface plasmon resonance (PSPR), which is generated in semi-infinitely continuous metal films.[19] Furthermore, the sensitivity of LSPR immunosensors is reduced considerably during the activation steps of the sensor surfaces such as functionalization of the metal surfaces, immobilization of capture probes, and reduction of nonspecific binding on the chip surface. For example, triangular Ag nanoparticles with no adsorbate overlayer (191 nm RIU^{-1}) and surfaces modified with a monolayer of $CH_3(CH_2)_{15}SH$ (150 nm RIU^{-1}) exhibited different sensitivity to the bulk RI.[10] When large molecules as receptors were immobilized onto Au nanoisland chips, the sensitivity in detecting molecular binding events was observed to be noticeably low.[20−22] Van Duyne's group has demonstrated alternative strategies for improving the LSPR sensitivity/detection limit based on the sandwich assay format.[10,11] This approach increases the additionally effective change in RI near the metal nanostructures *via* macromolecules[11] or plasmonic resonance coupling.[10] In addition, it has been reported previously that enzyme-catalyzed precipitation leads to a large change in RI at the flat surface of metal films in SPR.[23,24]

In this study, we demonstrate a new approach to an ultrasensitive LSPR immunosensor, in which enzyme-catalyzed precipitation on long-range ordered nanostructures is introduced as an enhancing method after the binding between PSA (~36 kDa) and its alkaline phosphatase (ALP)-tagged detection antibody. Since the plasmon field near 3-D metal nanostructures in LSPR is concentrated mainly within the range of a few tens of nanometers from the metal surfaces, the dense adsorption of the precipitate with a high dielectric constant in close proximity to the metal surfaces is expected to be more effective in inducing large changes in the detection signal than in SPR. Furthermore, from the viewpoint of application, enzyme−antibody conjugates have an advantage over NP−antibody conjugates which have still several limiting factors, such as nonspecific adsorption or binding, size variation, aggregation, and lack of stability.[3] Elliptical Au nanodisk arrays with a large area are fabricated onto a glass substrate by thermal nanoimprint lithography (NIL) with a laser interference lithography-assisted stamp. As an efficient postprocess of NIL, such as removing the residual polymer layer and creating an undercut of the patterned polymer, a tilted evaporation method is employed on imprinted resin patterns at the scale of a wafer. Finally, the optically anisotropic properties are analyzed in a PDMS fluidic system with a transmission LSPR device for the application to an LSPR-based nanobiosensor.

RESULTS AND DISCUSSION

Fabrication of elliptical Au nanodisk arrays on a glass substrate is schematically illustrated in Figure 1. In this study, the nanodisk array pattern on a Si stamp was transferred onto a glass wafer by thermal NIL and subsequent processes (tilted evaporation, O_2 plasma etching, metal deposition, lift-off) with high fidelity. A wafer-scaled stamp was fabricated by using laser interference lithography (LIL). It is well-known that LIL is a maskless technology that allows uniform and periodic submicrometer patterns over very large areas. A Si stamp was obtained at low cost, by LIL patterning and subsequent Si dry etching with short processing time (Figure 2A). In general, anisotropic reactive ion etching (RIE) and bilayer lift-off are utilized to remove a residual polymer layer in the process of transferring imprinted nanopatterns to metal nanostructures on a substrate in NIL.[16,18,25] It should be noted that the imprinting and/or the etching process is likely to cause slightly beveled sidewalls or round edges of the imprinted polymer, resulting in lift-off failure. However, in this study, metal masks created by tilted evaporation could protect perfectly the edges of the resin from being etched and produced an undercut in the sidewalls of the imprinted structures during O_2 plasma etching. As a result, we were able to easily transfer the pattern of the stamp to the metal nanodisk arrays on the glass wafer. Figure 2B shows that the size (long-axis and short-axis lengths; l_l and l_s) and pitch of the prepared elliptical Au nanodisk arrays on a glass substrate are defined by the dimensions of the stamp. The average l_l, l_s, and pitch of the Au nanodisk arrays were 162, 105, and 340 nm, respectively. The coefficient of variation (CV) for the size was less than 5%, indicating that the elliptical Au nanodisk arrays were fabricated with good uniformity. This result shows that our implementation including NIL is an effective way to fabricate nanostructures with a long-range order in a wafer scale.

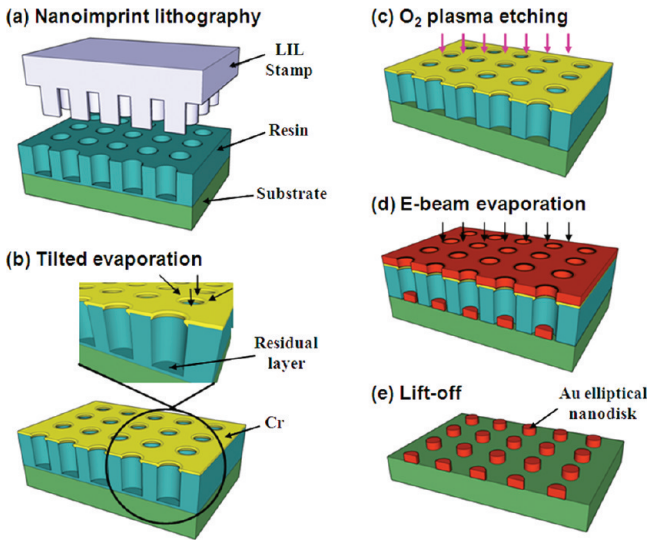

Figure 1. Fabrication of Au nanodisk arrays using nanoimprint lithography (NIL). (a) Imprinting the elliptical Au nanodisk arrays. (b) Depositing the mask layer of Cr by tilted evaporation to create an undercut. (c) Removing the residual layer by O_2 plasma etching. (d) Evaporating 1 nm Ti/20 nm Au film. (e) Lifting off the imprint resin.

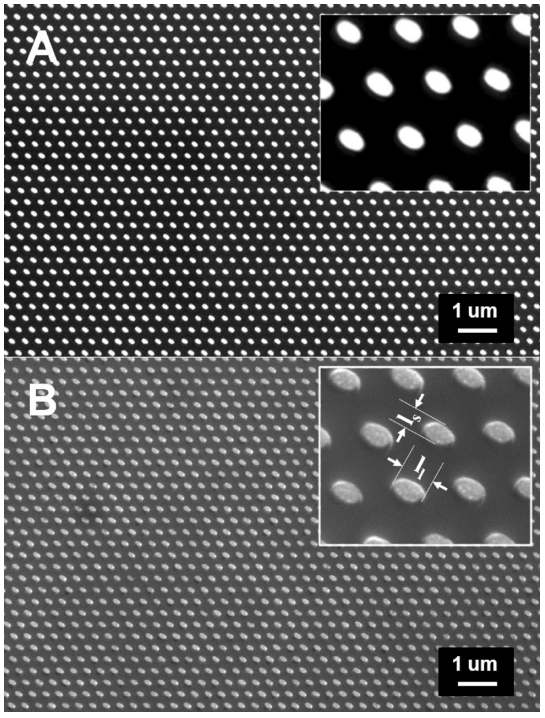

Figure 2. SEM images of (A) the array pattern of the elliptical Si nanopillars on an LIL stamp, and (B) the array pattern of elliptical Au nanodisks fabricated on a glass wafer.

The elliptical Au nanodisks show two extinction peaks due to their geometric anisotropy. Figure 3A shows the extinction spectrum of the Au nanodisk array on the glass wafer observed by using unpolarized light in air. This indicates that the nanodisk arrays exhibited two peaks in the visible and near-IR ranges. To provide a qualitative description of the experimental results, the theoretical analysis was performed using the discrete dipole approximation (DDA) method[26] (see the calculation details in the Supporting Information). As the result of the calculation, it was found that the former corresponds to the resonant response to the short axis of the elliptical nanodisks (s-peak, Figure 3B) and the latter to its long axis (l-peak, Figure 3C). In addition, the peak positions of the extinction maximum varied from 630 to 830 nm on both the theoretical analysis and the experimental results, depending on the polarization directions (see Figures S1 and S2 in the Supporting Information).

To analyze the sensing characteristics of elliptical Au nanodisk arrays on glass as an LSPR sensor, we examined briefly their sensitivity to the bulk RI. The sensitivities for both s-peak and l-peak were experimentally determined by the slope of a linear fit on the plot of LSPR peak wavelength in response to the bulk RI using aqueous solutions containing 0−60% glycerol, resulting in 167 and 327 nm RIU^{-1}, respectively (Figure 3D).

It is known that PSA is an important serum marker for the diagnosis of prostate cancer and should be detected at physiological (<4 ng mL^{-1}) and clinical (4−10 ng mL^{-1}) levels.[27] The modification of MUA (10 mM) on the bare Au nanodisk arrays and subsequent immobilization of capture antibodies (0.1 mg mL^{-1} monoclonal anti-PSA) induced total 19.1 and 28 nm average shifts in the s-peak and l-peak wavelength of the LSPR band, respectively. However, when the peak shifts of the LSPR band were observed during the binding event of PSA onto anti-PSA, a slight shift ($\Delta\lambda_{max} = 2$ nm) in the l-peak was detected only at a concentration of 2.8 nM PSA. No significant peak shifts ($\Delta\lambda_{max} < 1$ nm) were detected at PSA concentrations lower than 10 ng mL^{-1} (280 pM) for both the s-peak and l-peak when the baseline for LOD was defined as three times the instrumental noise. In addition, even the subsequent binding event of the detection antibody−enzyme conjugate could not cause a significant change in the LSPR signal.

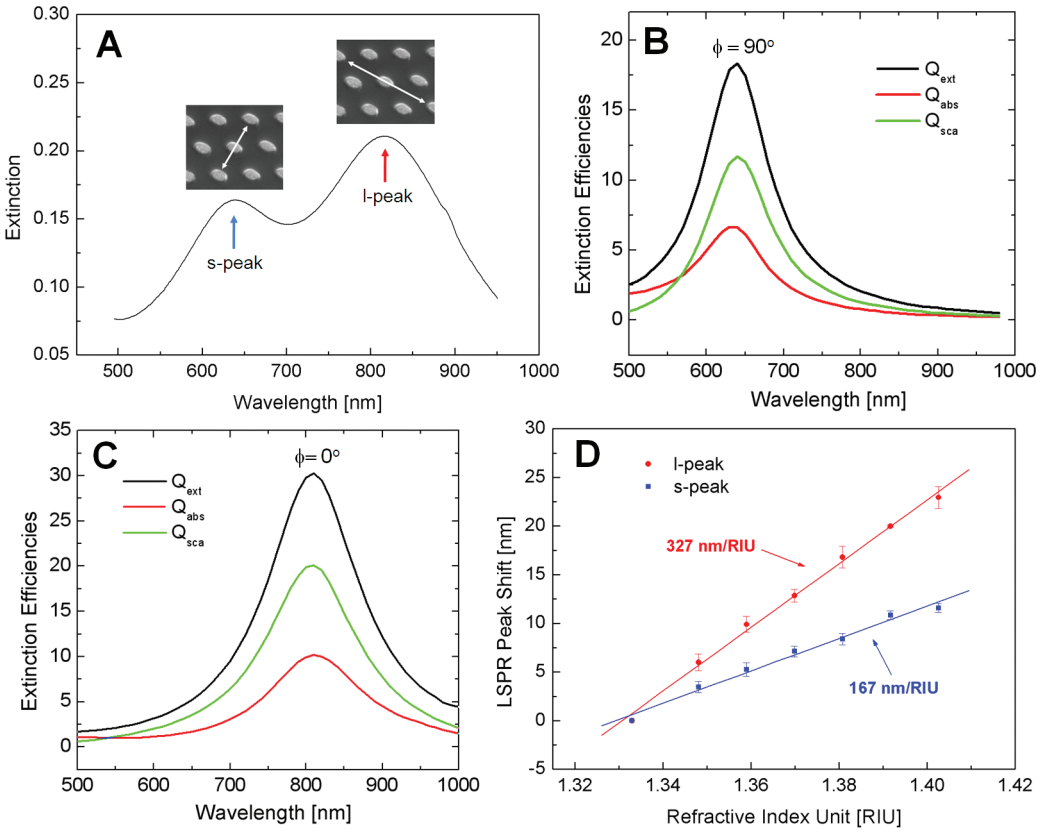

Figure 3. (A) Experimental extinction spectrum of as-prepared elliptical Au nanodisk arrays, including s-peak and l-peak. The theoretical results of an elliptical Au nanodisk analyzed by DDA, exhibiting (B) s-peaks and (C) l-peaks (ϕ: the poarization direction of the incident light against the long axis of the Au nanodisk). (D) Sensitivity to the bulk RI for s-peak/l-peak of the prepared elliptical Au nanodisk arrays, measured in the transmission mode.

To fully understand these phenomena, it is worth examining the fundamental characteristics of the LSP field in metal 3-D nanostructures. The amplitude of the LSP field is double-exponentially attenuated in the direction normal to the metal surface, so that the penetration depth of the LSP field in metal 3-D nanostructures is approximately 25 nm.[28] More specifically, the LSP field is distributed mainly in the short-range regions (~5−6 nm) from the metal surface.[10] It was experimentally confirmed by a layer-by-layer deposition of polyelectrolyte that the Au nanorods are most sensitive within the first 10 nm of the surface.[14] For this reason, the analyte molecules adsorbed on the surface of Au nanodisks that had been functionalized with large antibodies (~15 nm) and linkers (~2 nm) are hardly detectable, even though they are still in the sensing depth of the LSP field. Therefore, the larger the size of immobilized antibodies, the lower the sensitivity of label-free detection of target molecules.

As shown in Figure 4, no significant shifts in both s-peak and l-peak wavelength of the LSPR band were observed at PSA concentrations lower than 280 pM, until the enzymatic precipitation was introduced. Even at a concentration of 2.8 nM PSA, label-free detection of PSA was found to be difficult (see Figure S3 in the Supporting Information). On the other hand, the precipitation reaction led to dramatically large shifts over a wide range of PSA concentrations, so that even the binding of 10 pg mL^{-1} (280 fM) PSA in 0.1% BSA/PBS was found to be detectable as 4.7 and 5.5 nm in the s-peak and l-peak shifts, respectively (see Table S1 in the Supporting Information).

Figure 5A displays a SEM image of the nanodisk arrays after binding of 2.8 nM PSA and the precipitation reaction finally performed. It was observed that the precipitates were located just around the nanodisks, providing additional information that the capture antibody was immobilized efficiently only on the Au nanodisks, *via* the self-assembled monolayers of MUA on the metal surfaces. Furthermore, the nonspecific binding on the glass surface of PSA and enzyme−antibody conjugates appeared to be practically negligible. A compositional analysis using energy-dispersive X-ray (EDX) spectroscopy also shows that the precipitates on the Au nanodisks were the products due to the enzymatical reaction of the BCIP/NBT substrate (see Figure S4 in the Supporting Information). To further investigate the morphological change of the nanodisks and obtain quantitative data of the precipitates, we performed 3-D topographical measurements by using atomic force microscopy (AFM) (see Figures S5 and S6 in the Supporting Information). We could see the difference in the size and shape of the nanodisks

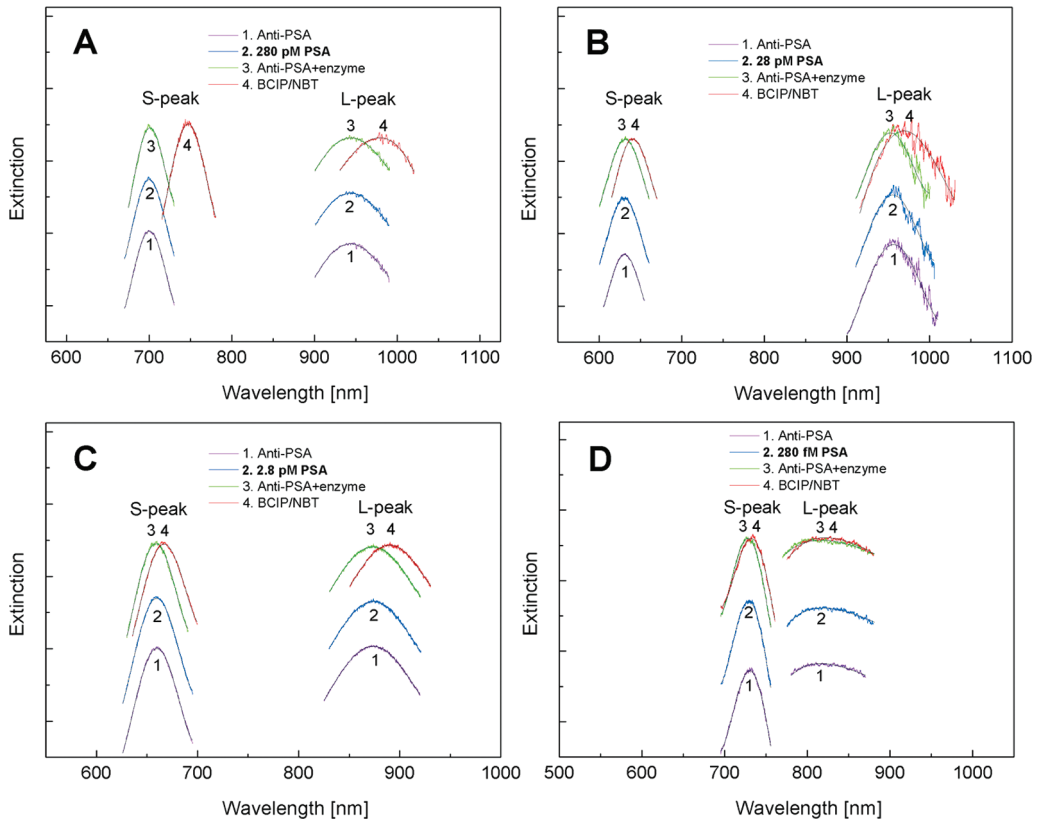

Figure 4. LSPR spectra according to each binding step after the binding of (A) 280 pM, (B) 28 pM, (C) 2.8 pM, and (D) 280 fM PSA in 0.1% BSA/PBS.

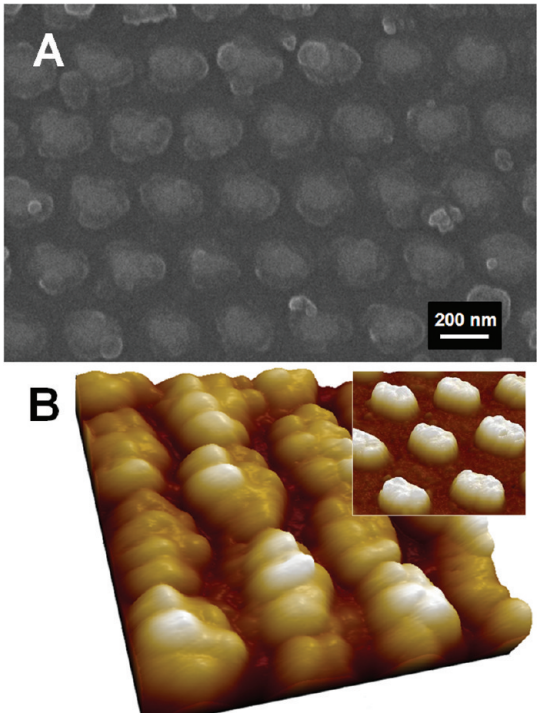

Figure 5. (A) SEM image and (B) AFM image of elliptical Au nanodisk arrays after the precipitation reaction with the binding of 2.8 nM PSA. The inset shows an AFM image of the nanodisk array just before the precipitation reaction.

between the samples before and after the precipitation reaction (2.8 nM PSA) in Figure 5B; this could be observed even with the binding of 280 pM PSA (see Figure S7 in the Supporting Information). The nanodisks covered with the precipitates had bumpy surfaces with different heights, ranging from 34.1 to 52.2 nm (2.8 nM PSA) and from 28.5 to 39.7 nm (280 pM PSA), respectively. The large difference in total height on the same nanodisk can be attributed to the inhomogeneous precipitation over the metal surface, resulting from the random distribution and orientation of biomolecules. The average heights of the nanodisks increased by 11.4 nm (2.8 nM PSA) and 2.1 nm (280 pM PSA) after the precipitation reaction, resulting in 37.1 and 18.0 nm red shifts in the s-peak wavelength of the LSPR band, as well as 48.1 and 29.1 nm in the l-peak, respectively. Compared to biomolecules such as PSA and the antibody−enzyme conjugate, even a small amount of precipitate located within the LSP field could cause the relatively large red shifts in both of the peaks. This results from the fact that the precipitate, including bromine and chlorine, has a high dielectric constant and is densely adsorbed in close proximity to the metal surfaces. Therefore, this precipitation approach could be a simple and effective way to improve the sensitivity of LSPR sensors.

Moreover, since the catalytic efficiency of enzyme−substrate reaction is high, the reaction time can be reduced to a few minutes. We measured the change in the LSPR peak wavelength in real time during the enzyme-catalyzed reaction (5 μL min^{-1} flow rate for

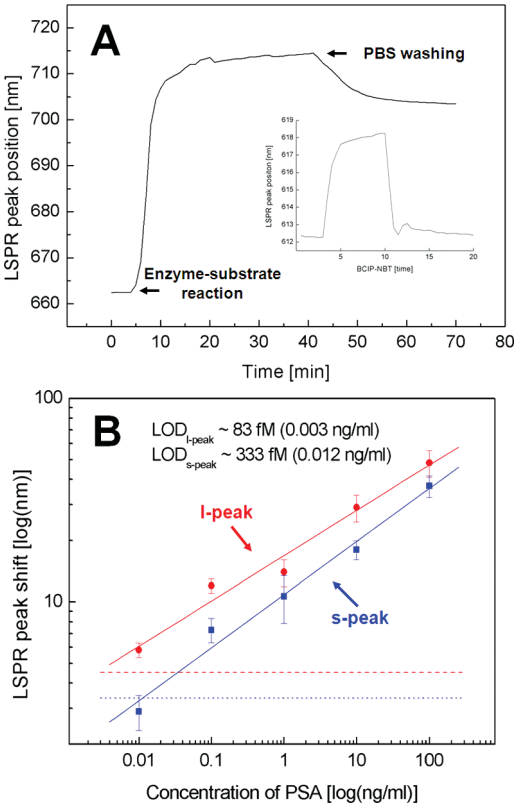

Figure 6. (A) Peak positions of the LSPR band as a function of time during an enzyme-catalyzed precipitation reaction (5 μL min^{-1} flow rate, 40 min) and subsequent PBS washing (100 μL min^{-1} flow rate, 30 min) with the binding of 2.8 nM PSA. The inset shows the reaction of the substrate solution and PBS washing without both the binding of PSA and the reaction of enzyme–antibody conjugates. (B) Calibration curve for the precipitation reaction on the Au nanodisk surface. All experiments were repeated three times. The error bars represent the standard deviation of LSPR peak shifts according to each concentration; the red dash and blue dot lines represent the sum of the average shift and the standard deviation of the l-peak and s-peak shifts of the LSPR band in a negative control experiment, without PSA binding, respectively.

40 min) and subsequent PBS washing (100 μL min^{-1} flow rate for 30 min) after the binding of 2.8 nM PSA (Figure 6A). The change in the peak position reached approximately 90% of the maximum value within 10 min after the injection of the substrate solution. In addition, most of the weak binding of the precipitate induced by nonspecific reaction was removed within 5 min. The BCIP/NBT solution left in the PDMS chamber was flushed out at the same time. The inset in Figure 6A shows the experimental result on any possible effect of self-precipitation or adsorption of the substrate solution. When the precipitation reaction and subsequent PBS washing were carried out without the PSA and antibody–enzyme conjugates, the peak position of LSPR band returned to the initial position after PBS washing for 3 min.

Finally, a negative control experiment was performed to determine LOD, defined as the lowest concentration from which the sensor response was distinguished statistically (Figure 6B). The LOD in the experiments for label-free detection of LSPR sensors is generally determined, based on three times the standard deviation of the instrumental noise as a baseline.[10] However, this baseline may not be acceptable in the sandwich assay format because even a little nonspecific binding of the detection antibody conjugates can be highly amplified by the enzymatic reactions. Indeed, a small amount of nonspecific binding was observed in our control experiments performed without PSA when the baseline for LOD was defined as the average shift plus standard deviation.[14] These values were 3.37 and 4.5 nm for the s-peak and l-peak, respectively. On the basis of this actual control experiment, the LOD was determined to be ~0.012 ng mL^{-1} (333 fM) and ~0.003 ng mL^{-1} (83 fM), which means that LOD was enhanced ~10^5 times by enzymatic signal amplification over that obtained with the label-free experiment. This is a better result than the previous results, which have the detection limit of 1.0 ng mL^{-1} in diluted serum samples[29] and 0.15 ng mL^{-1} in 3% BSA in PBS samples[30] using commercial SPR sensors, with colloidal gold enhanced sandwich assays. Moreover, we expect that LOD can be improved much more *via* strategies for the more efficient reduction of nonspecific binding on metal surfaces.

CONCLUSIONS

We have demonstrated the fabrication of elliptical Au nanodisk arrays *via* thermal NIL for an LSPR sensor. Long-range ordered nanodisk arrays can be fabricated reproducibly using low-cost lithographic methods (LIL and NIL) that could allow high-throughput fabrication of LSPR biosensor chips. The Au elliptical nanoarrays fabricated on glass have an l-peak response that is more sensitive to the bulk RI than that of the s-peak in the LSPR spectra. For application to clinical PSA diagnostics, the peak shift of the LSPR band has been amplified by the enzyme-catalyzed BCIP/NBT precipitation, resulting in a remarkable enhancement of the detection limit that is far under the diagnostic level of 4–10 ng mL^{-1} PSA. The enzyme-catalyzed precipitation method in the LSPR sensor could be extended to detect analytes with low molecular weight and other clinical biomarkers at low concentrations in actual clinical samples.

EXPERIMENTAL SECTION

Materials. Bovine serum albumin (BSA), *N*-hydroxysuccinimide (NHS), 11-mercaptoundecanoic acid (MUA), ethanolamine, straptavidin–alkaline phosphatase (ALP), 5-bromo-4-chloro-3-indolyl phosphate *p*-toluidine (BCIP), and nitro blue tetrazolium (NBT) were purchased from Sigma-Aldrich (St. Louis, MO).

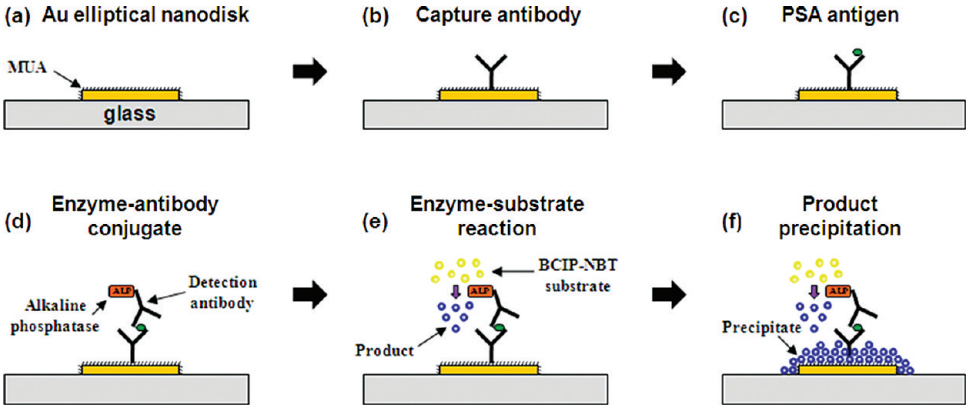

Figure 7. Schematic illustration of PSA detection procedure, including surface modification and biochemical binding reactions. (a) Modification with MUA. (b) Immobilization of the PSA antibody. (c) Binding of PSA to the antibody. (d) Sandwich binding of alkaline phosphatase−detection antibody conjugate to PSA. (e) Enzymatic reaction of the BCIP/NBT substrate. (f) Product precipitation on the nanodisk.

Recombinant human prostate-specific antigen (PSA), monoclonal capture antibodies, and biotinylated polyclonal detection antibodies were purchased from R&D systems (Minneapolis, MN). Sodalime glass wafers were obtained from Buysemi (Suwon, Gyeonggido, Korea), and 1-ethyl-3-(3-dimethylaminopropyl)-carbodiimide (EDC) was purchased from ThermoFisher Scientific (Waltham, MA). Glycerol (SigmaUltra, ≥99%) was purchased from Sigma-Aldrich, Inc.

Fabrication of Elliptical Au Nanodisk Arrays. Au nanodisk arrays on a glass wafer were fabricated by the serial processes of NIL, tilted evaporation, O_2 plasma etching, metal deposition, and lift-off. First, a Si stamp with nanoscale features was prepared by laser interference lithography (LIL), and then the surface of the Si stamp was modified with hydrophobic chemicals for easy release of the stamp from the resin after imprinting. The stamp with nanopillar array patterns was pressed on a thermally curable resin using a thermal NIL machine, as shown in Figure 1. The resin (mr_I8030E, Micro Resist Technology GmbH, Germany) was diluted with its thinner at a ratio of 3:2 and spin-coated on a glass wafer at 3000 rpm for 30 s, representing the resin thickness of 170 nm. The imprinting was performed under the pressure of 50 bar at 180 °C for 10 min (see Figure S8 in the Supporting Information) and maintained until the temperature decreased below 50 °C (Figure 1a). To protect a top layer of the patterned resin from O_2 plasma etching, a 2 nm layer of chromium was deposited at a tilted angle of about 70° four times in different directions in an e-beam evaporator (Figure 1b). The residual layer was removed by O_2 plasma etching (Plasma Finish, Wertheim, Germany) at an O_2 flow rate of 300 mL min^{-1} and 300 W power for 6 min (Figure 1c). Finally, a Ti/Au layer (1 nm/20 nm) was deposited by e-beam evaporation (Figure 1d), and lift-off was achieved with ultrasonic agitation in acetone (Figure 1e).

Modification of the Nanodisk Surface and Biochemical Binding. Figure 7 shows the surface modification of the nanodisks and the binding procedure for the detection of PSA. (a) The prepared Au nanodisk array chips were treated in a "piranha solution" (H_2SO_4/H_2O_2 = 3:1) to clean the surface of the nanodisks, followed by rinsing with deionized (DI) water, and dried under a stream of nitrogen. The cleaned nanodisk chips were immersed in an ethanol solution containing 10 mM MUA for 12 h. Subsequently, the terminal carboxylate groups of MUA surfaces were activated in a solution of 0.1 M EDC and 0.025 M NHS in DI water for 15 min. (b) To immobilize the capture antibodies on the activated MUA surface, the chips were incubated in phosphate-buffered saline (PBS, pH 7.4) containing 0.1 mg mL^{-1} of anti-PSA antibodies for 1 h. Nonspecific binding was prevented by using 1.0 M ethanolamine/HCl (pH 8.5) for 15 min and then 10 mg mL^{-1} of BSA in PBS for 1 h. (c) The antigen−antibody reaction was carried out for 1 h in PBS containing 1 mg mL^{-1} BSA and varying concentrations (100, 10, 1, 0.1, 0.01 ng mL^{-1}) of recombinant PSA. (d) The sandwich assay was performed for 30 min in a solution of 1 μg mL^{-1} biotinylated anti-PSA and 1 μg mL^{-1} streptavidin−alkaline phosphatase in 1 mg mL^{-1} BSA/PBS. (e) The enzyme-catalyzed precipitation reaction was triggered by the addition of 0.1 M BCIP and 1 mg mL^{-1} NBT in 0.1 M Tris-HNO_3 at pH 9.8 for 30 min. (f) Finally, the reduction of the BCIP/NBT substrate yielded insoluble precipitates on the nanodisk surfaces and increased the change in the LSPR signal.

Transmission LSPR Spectroscopy through a PDMS Fluidic Channel. The LSPR spectrum of Au nanodisk arrays was collected by using a white light source (KL 1500, Carl Zeiss) and a fiber-optic spectrometer (HR4000, OceanOptics) through a polydimethylsiloxane (PDMS) fluidic channel in the transmission mode. The PDMS chamber whose dimension was 2 mm × 2 mm × 1 mm (width × length × height) and was molded on a poly(methyl methacrylate) (PMMA) master. A 1:11 mixture of a curing agent and PDMS monomers (Dow Corning, Michigan, USA) was poured on the mold and baked in an oven for 4 h after degassing. The LSPR spectra were measured after every process for the biochemical binding and the subsequent washing. Sample solutions were delivered by using a syringe pump in the suction mode. The flow rate was 5 and 100 μL min^{-1} for molecular binding and washing, respectively. The peak wavelength of the LSPR band was determined by applying a fifth order polynomial fit.

Acknowledgment. This research was supported by a grant from the Center for Nanoscale Mechatronics & Manufacturing, one of the 21st Century Frontier Research Programs (08K1401-00313), a grant from the Converging Research Center Program through the National Research Foundation of Korea (NRF) (2009-0082335), which are supported by the Ministry of Education, Science and Technology, KOREA, and a grant from the KRIBB Initiative Research Program (KRIBB, Korea).

Supporting Information Available: Calculation of theoretical extinction of nanodisk array, the compositional analyses of the precipitates and AFM analysis, *etc*. This material is available free of charge *via* the Internet at http://pubs.acs.org.

REFERENCES AND NOTES

1. Stewart, M.; Anderton, C.; Thompson, L.; Maria, J.; Gray, S.; Rogers, J.; Nuzzo, R. Nanostructured Plasmonic Sensors. *Chem. Rev.* **2008,** *108*, 494–521.
2. Haes, A.; Duyne, R. Preliminary Studies and Potential Applications of Localized Surface Plasmon Resonance Spectroscopy in Medical Diagnostics. *Expert Rev. Mol. Diagn.* **2004,** *4*, 527–537.
3. Gomez-Hens, A.; Fernandez-Romero, J.; Aguilar-Caballos, M. Nanostructures as Analytical Tools in Bioassays. *Trends Anal. Chem.* **2008,** *27*, 394–406.
4. Haynes, C.; Van Duyne, R. Nanosphere Lithography: A Versatile Nanofabrication Tool for Studies of Size-Dependent Nanoparticle Optics. *J. Phys. Chem. B* **2001,** *105*, 5599–5611.

5. Kelly, K.; Coronado, E.; Zhao, L. L.; Schatz, G. C. The Optical Properties of Metal Nanoparticles: The Influence of Size, Shape, and Dielectric Environment. *J. Phys. Chem. B* **2003,** *107*, 668–677.
6. Chan, G. H.; Zhao, J.; Schatz, G. C.; Duyne, R. P. V. Localized Surface Plasmon Resonance Spectroscopy of Triangular Aluminum Nanoparticles. *J. Phys. Chem. C* **2008,** *112*, 13958–13963.
7. Anker, J.; Hall, W.; Lyandres, O.; Shah, N.; Zhao, J.; Van Duyne, R. Biosensing with Plasmonic Nanosensors. *Nat. Mater.* **2008,** *7*, 442–454.
8. Stewart, M. E.; Mack, N. H.; Malyarchuk, V.; Soares, J. A. N. T.; Lee, T.-W.; Gray, S. K.; Nuzzo, R. G.; Rogers, J. A. Quantitative Multispectral Biosensing and 1D Imaging Using Quasi-3D Plasmonic Crystals. *Proc. Natl. Acad. Sci. U.S.A.* **2006,** *103*, 17143–17148.
9. Stewart, M. E.; Yao, J.; Maria, J.; Gray, S. K.; Rogers, J. A.; Nuzzo, R. G. Multispectral Thin Film Biosensing and Quantitative Imaging Using 3D Plasmonic Crystals. *Anal. Chem.* **2009,** *81*, 5980–5989.
10. Haes, A. J.; Van Duyne, R. P. A Nanoscale Optical Biosensor: Sensitivity and Selectivity of an Approach Based on the Localized Surface Plasmon Resonance Spectroscopy of Triangular Silver Nanoparticles. *J. Am. Chem. Soc.* **2002,** *124*, 10596–10604.
11. Haes, A.; Chang, L.; Klein, W.; Van Duyne, R. Detection of a Biomarker for Alzheimer's Disease from Synthetic and Clinical Samples Using a Nanoscale Optical Biosensor. *J. Am. Chem. Soc.* **2005,** *127*, 2264–2271.
12. Zheng, Y.; Juluri, B.; Mao, X.; Walker, T.; Huang, T. Systematic Investigation of Localized Surface Plasmon Resonance of Long-Range Ordered Au Nanodisk Arrays. *J. Appl. Phys.* **2008,** *103*, 014308.
13. Lucas, B.; Kim, J.; Chin, C.; Guo, L. Nanoimprint Lithography Based Approach for the Fabrication of Large-Area, Uniformly-Oriented Plasmonic Arrays. *Adv. Mater.* **2008,** *20*, 1129–1134.
14. Marinakos, S.; Chen, S.; Chilkoti, A. Plasmonic Detection of a Model Analyte in Serum by a Gold Nanorod Sensor. *Anal. Chem.* **2007,** *79*, 5278–5283.
15. Lee, S.; Mayer, K. M.; Hafner, J. H. Improved Localized Surface Plasmon Resonance Immunoassay with Gold Bipyramid Substrates. *Anal. Chem.* **2009,** *81*, 4450–4455.
16. Chou, S.; Krauss, P.; Renstom, P. Nanoimprint Lithography. *J. Vac. Sci. Technol., B* **1996,** *14*, 4129–4133.
17. Zankovych, S.; Hoffmann, T.; Seekamp, J.; Bruch, J.; Torres, C. Nanoimprint Lithography: Challenges and Prospects. *Nanotechnology* **2001,** *12*, 91–95.
18. Hu, W.; Wilson, R.; Xu, L.; Han, S.; Wang, S. Patterning of High Density Magnetic Nanodot Arrays by Nanoimprint Lithography. *J. Vac. Sci. Technol., A* **2007,** *25*, 1294–1297.
19. Haes, A.; Van Duyne, R. A Unified View of Propagating and Localized Surface Plasmon Resonance Biosensors. *Anal. Bioanal. Chem.* **2004,** *379*, 920–930.
20. Shin, Y.-B.; Lee, J.-M.; Park, M.-R.; Kim, M.-G.; Chung, B. H.; Pyo, H.-B.; Maeng, S. Analysis of Recombinant Protein Expression Using Localized Surface Plasmon Resonance (LSPR). *Biosens. Bioelectron.* **2007,** *22*, 2301–2307.
21. Kim, H.; Jin, S.; Lee, S.; Kim, M.; Shin, Y. Detection of Biomolecular Binding through Enhancement of Localized Surface Plasmon Resonance (LSPR) by Gold Nanoparticles. *Sensors* **2009,** *9*, 2334–2344.
22. Frederix, F.; Friedt, J.; Choi, K.; Laureyn, W.; Campitelli, A.; Mondelaers, D.; Maes, G.; Borghs, G. Biosensing Based on Light Absorption of Nanoscaled Gold and Silver Particles. *Anal. Chem.* **2003,** *75*, 6894–6900.
23. Kim, M.; Shin, Y.; Jung, J.; Ro, H.; Chung, B. Enhanced Sensitivity of Surface Plasmon Resonance (SPR) Immunoassays Using a Peroxidase-Catalyzed Precipitation Reaction and Its Application to a Protein Microarray. *J. Immunol. Methods* **2005,** *297*, 125–132.
24. Li, Y.; Lee, H.; Corn, R. Detection of Protein Biomarkers Using RNA Aptamer Microarrays and Enzymatically Amplified Surface Plasmon Resonance Imaging. *Anal. Chem.* **2007,** *79*, 1082–1088.
25. Faircloth, B.; Rohrs, H.; Tiberio, R.; Ruoff, R.; Krchnavek, R. Bilayer, Nanoimprint Lithography. *J. Vac. Sci. Technol., B* **2000,** *18*, 1866–1873.
26. Draine, B. T.; Flatau, P. J. Discrete-Dipole Approximation for Scattering Calculation. *J. Opt. Soc. Am. A* **1994,** *11*, 1491–1499.
27. Healy, D.; Hayes, C.; Leonard, P.; McKenna, L.; O'Kennedy, R. Biosensor Developments: Application to Prostate-Specific Antigen Detection. *Trends Biotechnol.* **2007,** *25*, 125–131.
28. Yonzon, C.; Stuart, D.; Zhang, X.; McFarland, A.; Haynes, C.; Van Duyne, R. Towards Advanced Chemical and Biological Nanosensors—An Overview. *Talanta* **2005,** *67*, 438–448.
29. Huang, L.; Reekmans, G.; Saerens, D.; Friedt, J.; Frederix, F.; Francis, L.; Muyldermans, S.; Campitelli, A.; Hoof, C. Prostate-Specific Antigen Immunosensing Based on Mixed Self-Assembled Monolayers, Camel Antibodies and Colloidal Gold Enhanced Sandwich Assays. *Biosens. Bioelectron.* **2005,** *21*, 483–490.
30. Besselink, G.; Kooyman, R.; van Os, P.; Engbers, G.; Schasfoort, R. Signal Amplification on Planar and Gel-Type Sensor Surfaces in Surface Plasmon Resonance-Based Detection of Prostate-Specific Antigen. *Anal. Biochem.* **2004,** *333*, 165–173.